A Volumetric Approach to Quantifying Region-to-Region White Matter Connectivity in Diffusion Tensor MRI

P. Thomas Fletcher, Ran Tao, Won-Ki Jeong, and Ross T. Whitaker

School of Computing, University of Utah, Salt Lake City, UT, USA

Abstract. In this paper we present a volumetric approach for quantitatively studying white matter connectivity from diffusion tensor magnetic resonance imaging (DT-MRI). The proposed method is based on a minimization of path cost between two regions, defined as the integral of local costs that are derived from the full tensor data along the path. We solve the minimal path problem using a Hamilton-Jacobi formulation of the problem and a new, fast iterative method that computes updates on the propagating front of the cost function at every point. The solutions for the fronts emanating from the two initial regions are combined, giving a voxel-wise connectivity measurement of the optimal paths between the regions that pass through those voxels. The resulting high-connectivity voxels provide a volumetric representation of the white matter pathway between the terminal regions. We quantify the tensor data along these pathways using nonparametric regression of the tensors and of derived measures as a function of path length. In this way we can obtain volumetric measures on white-matter tracts between regions without any explicit integration of tracts. We demonstrate the proposed method on several fiber tracts from DT-MRI data of the normal human brain.

1 Introduction

Diffusion tensor magnetic resonance imaging (DT-MRI) has the ability to reveal *in vivo* properties of white matter tissue in the human brain. As such, DT-MRI is becoming a powerful technique for clinical studies of white matter abnormalities in neurological disorders as well as studies of normal brain development. The usefullness of diffusion imaging relies on the fact that the motion of water is impeded in directions that are not parallel to the axons. In DT-MRI a diffusion tensor at each voxel gives an estimated model of the pattern of water diffusion aggregated over a point-spread function of the measurements. The neural fiber orientation is typically inferred from the principal eigenvector of the diffusion tensor, which is the direction of highest probability of water motion.

Clinical studies have been mostly limited to analysis of white matter properties in a region of interest (ROI) [1,2]. Typically, statistics are computed on derived tensor measurements, such as fractional anisotropy (FA) or mean diffusivity (MD). This analysis is done either on a voxel-by-voxel basis or as an

N. Karssemeijer and B. Lelieveldt (Eds.): IPMI 2007, LNCS 4584, pp. 346–358, 2007.

aggregate measurement within the ROI. Because of the complexity of the diffusion tensor data, registration of images to a common atlas for voxelwise statistics is particularly problematic. Recent work has explored statistical analysis of derived measures [3,4] and also of the entire tensors [5] along fiber pathways.

Much of the work in DT-MRI connectivity focuses on fiber tractography [6], in which streamlines are computed, by forward integration from a seed point, of the field of vectors defined by the principal eigenvector of the tensor at each point (interpolated between voxels), and where the twofold ambiguity of eigenvector directions is resolved by the continuity of paths. While tractography is an excellent tool for visualization of white matter pathways, it is not ideal for quantitative analysis for several reasons. First, imaging noise can cause fiber tracts to stray due to accumulating errors in the integration. The second issue is partial voluming. The finite size of a voxel measurement at fiber crossings (combined with sensor noise) can cause the direction of the major eigenvector to be ambiguous, further misleading the streamlines. This problem is aggravated by the fact that streamlines are often computed, displayed, and analyzed at subvoxel resolution—suggesting a level of precision that is not warranted by the data. Finally, region-to-region analysis with conventional tractography is challenging, because there is no way to steer tracts from a seed point toward a particular target region. To address these problems, several researchers propose tractography algorithms that rely on a stochastic integration, in which flow vector are chosen from a distribution around the principal eigenvector. These stochastic techniques can be combined with Monte-Carlo simulations, which may include tens of thousands of paths from a single seed, of which only a small fraction will typically reach the target [7,8,9,10].

Several Hamilton-Jacobi (H-J) methods for white matter connectivity have been proposed to overcome some of the difficulties arising in tractography. These methods compute the cost of the shortest path from a seed region to every pixel in the volume (usually a white-matter mask). This cost function consists of an integral that depends on path position and orientation, and typically penalizes paths that do not agree with the tensors. These H-J formulations result in first-order partial differential equations (PDEs) which model evolving fronts whose speeds are determined by information from the diffusion tensor. These methods are inherently more robust to noise in the diffusion weighted measurements than standard tractography. Parker et al. [11] evolve a front with speed related to the inner product of the front normal with the principal eigenvector of the tensor. O'Donnell et al. [12] propose using the diffusion tensor as a Riemannian metric in the image domain and compute a front representing arrival time of geodesics beginning at a single seed point. Connectivity to that point is defined as a ratio of Euclidean path length to Riemannian distance. Jackowski et al. [13] use a speed derived as a function of the diffusivity magnitude in the front normal direction. They solve this Hamiltonian equation using a Lax-Friedrichs scheme, also beginning with an intial seed point. Pichon et al. [14] define a directionally dependent local cost function that extends the H-J framework to high-angular diffusion data. In all of these works, the end result is either a dense field of

connectivities to regions or a set of optimal paths emanating from a seed region, which are determined by integrating the characteristics of the PDEs.

In this paper we present a new method for quantifying white matter connectivity based on a H-J formulation, which we solve with a front propagating method. However, unlike previous H-J methods, which solve for the minimal cost of paths emanating from a single region, we formulate a cost for a very large number of paths *between* two regions. This results in a measure of region-to-region connectivity as well as a volumetric representation of the pathway between the two regions, without any explicit integration of individual paths. This approach is targeted to the study of white matter circuits between functional regions of the grey matter. We demonstrate the quantification of white matter properties, including both full tensor and derived measurements, along fiber pathways using nonparametric regression.

2 Region-to-Region Connectivity

Our formulation of region-to-region connectivity is based on the principle of minimal cost paths. Using information from the entire diffusion tensor, we construct a local cost function based the current position and directionality of a path. This leads to a first-order nonlinear PDE that computes the minimal cost from a starting region to each point in the image. Unlike previous front-propagation methods for DT-MRI, we then solve for minimal cost from a second target region. The two solutions are then combined, giving the minimal cost through each voxel of paths restricted to travel between the two target regions.

2.1 Minimum Cost Paths

Given a path $c : [a, b] \to \Omega$, where Ω is a compact image domain, we define the total cost of c as

$$E(c) = \int_a^b \psi(c(t), T(t))dt, \tag{1}$$

where $T(t) = c'(t)/\|c'(t)\|$ is the unit tangent vector of c. The total cost is defined as the integral of a *local cost function*, $\psi : \Omega \times S^1 \to \mathbb{R}$, where $\psi(x, v)$ gives the cost of moving in the unit direction $v \in S^1$ from the point $x \in \Omega$. We require that the local cost be symmetric, $\psi(x, v) = \psi(x, -v)$, which is generally consistent with the model of diffusion through passive media.

This metric in (1) allows for a wide range of cost functions ψ that incorporate tangents. Pichon et al. [14] describe the properties of this metric, the choices of ψ for high-angular diffusion data, and the relationship between this cost function and the corresponding *speed* that controls the motion of the wavefront in the H-J formulation. In this work we use a quadratic (bilinear) local cost function, with the understanding that all of the results in this paper generalize to high-angular data using the methods described in [14]. Thus we have

$$\psi(x, v) = v^T M^{-1}(x) v, \tag{2}$$

where $M(x)$ is a symmetric, positive-definite matrix defined at each point $x \in \Omega$.

The relationship between the measured diffusion tensor and M must be considered carefully. For instance, several researchers [12,15] use as their cost, the bilinear product with the inverse of the diffusion tensor itself. However, even in ideal situations (straight bundles of healthy axons) [16], the tensors are not be perfectly anisotropic, because of some degree of diffusion between or through cells. Thus, good measurements of tissue with relatively high FA, such as in the corpus collosum, might have values as low as 0.7, which would not offer sufficient penality for paths that cross the principal eigen directions. Because of this, the paths are relatively unconstrained by the diffusion tensors themselves, and solutions tend toward the shortest paths in the Euclidean sense, rather than following the white matter tracts. The same is true if we use the tensors directly in a second order PDE and model the diffusion of water from the tensors [12]—the resulting connectivities spread too easily outside of the paths defined by the principal eigenvectors, which limits their usefulness. On the other extreme, we could construct tensors from the principal eigenvectors that produce a virtually infinite penalty (zero speed) for all other directions. This, however, would ignore any meaningful differences between different tensor shapes, including the case of oblate tensors which are thought to represent fiber crossings and provide virtually equal evidence for all directions spanned by the first two eigenvectors.

One middle ground between these two extremes is to *sharpen* the tensor, which is done by raising it to a power α. This must be combined with a normalization, and for this work we normalize by the tensor volume. If we consider the sharpened tensor to be speed (in the H-J formulation), which gives low cost along the principal eigen directions, the cost is the inverse, and we have

$$M(x) = |D(x)|^{\frac{1}{3}} \left(\frac{D(x)}{|D(x)|^{\frac{1}{3}}} \right)^{\alpha}, \tag{3}$$

where $\alpha > 1$ is a constant and $|D(x)|$ denotes the determinant of $D(x)$. The sharpened tensor field M has the following properties:

1. If $D(x)$ has eigenvalues $\lambda_i(x)$, then $M(x)$ has eigenvalues $\lambda_i(x)^{\alpha}|D(x)|^{\frac{1-\alpha}{3}}$.
2. $|M(x)| = |D(x)|$ for all $x \in \Omega$, i.e., tensor volume is preserved.
3. If $D(x) = aI$, then $M(x) = D(x)$, in other words, isotropic tensors are left unchanged.

We can consider all paths emanating from a region $R_1 \subset \Omega$. Let $u_1(x)$ denote the minimal cost as defined by (1) over all paths beginning in the region R_1 and terminating at the point x. Then u_1 satisfies the first-order equation

$$\|\nabla u_1(x)\| = \psi\left(x, \nabla u / \|\nabla u\|\right), \tag{4}$$

with initial conditions $u_1(R_1) = 0$.

2.2 Costs Between Regions

While u_1 gives us a measure of the connectivity from the region R_1 to any point in the image, we would like to assess the specific connectivity to a second target

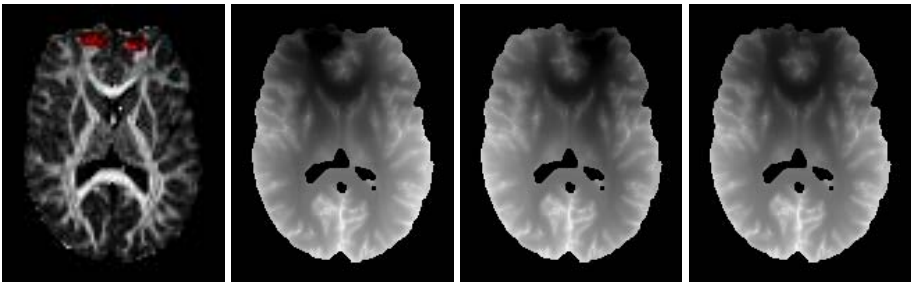

Fig. 1. An axial slice from the FA image with regions R_1 and R_2 highlighted (left). The cost functions u_1 and u_2 (middle two). The total cost function $u = u_1 + u_2$ (right).

region. To do this, we define a second region $R_2 \subset \Omega$ and corresponding minimal cost function u_2 also satisfying (4). Consider all paths beginning in the region R_1 and terminating in R_2. Now we define the *total cost function* for regions R_1 and R_2 to be $u(x) = u_1(x) + u_2(x)$. The value of $u(x)$ is the minimal cost of all paths between R_1 and R_2 *that are constrained to pass through* x. This is formalized in the following theorem.

Theorem 1. *Let $x \in \Omega$, and let Γ be the space of all paths $\gamma : [a_\gamma, b_\gamma] \to \Omega$ such that $\gamma(a_\gamma) \in R_1$ and $\gamma(b_\gamma) \in R_2$ and $\gamma(t) = x$ for some $t \in [a_\gamma, b_\gamma]$, then $u(x)$ satisfies*

$$u(x) = \min_{\gamma \in \Gamma} E(\gamma).$$

Proof. By definition of the path space Γ, we can break any path $\gamma \in \Gamma$ into a path γ_1 from R_1 to the point x and a path γ_2 from the point x to the region R_2. We thus have $E(\gamma) = E(\gamma_1) + E(\gamma_2)$. Because $u_1(x)$ minimizes the cost $E(\gamma_1)$ and $u_2(x)$ minimizes the cost $E(\gamma_2)$, $u(x) = u_1(x) + u_2(x)$ must also minimize the cost $E(\gamma)$. □

Thus, the function u assigns to each point x in the image the cost of that point being included in a pathway between regions R_1 and R_2. The construction of the total cost function u is demonstrated in Figure 1, showing a tract through the genu of the corpus callosum in DT-MRI data from a normal brain. If we assume a compact image domain Ω, then u must have a minimum value in Ω. As the next theorem shows, this minimal value is in fact achieved everywhere along the minimal cost path connecting the two regions.

Theorem 2. *Let $\gamma : [a, b] \to \Omega$ be the minimal total cost path with $\gamma(a) \in R_1$ and $\gamma(b) \in R_2$. Then u is constant along γ with $u(\gamma(t)) = E(\gamma)$ for all $t \in [a, b]$. Furthermore, $u(\gamma(t)) = \min_x u(x)$.*

Proof. Let $T(t) = \gamma'(t)/\|\gamma'(t)\|$ be the unit tangent vector of γ. Given any point $t_0 \in [a, b]$, we have $E(\gamma) = \int_a^{t_0} \psi(\gamma(t), T(t))dt + \int_{t_0}^b \psi(\gamma(t), T(t))dt$. Due to the symmetry of the local cost, $\psi(x, v) = \psi(x, -v)$, this implies that $E(\gamma) =$

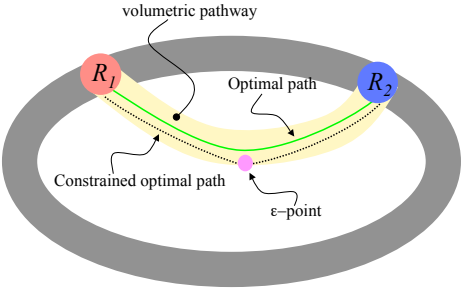

Fig. 2. Diagram of the volumetric connectivity framework

$\int_a^{t_0} \psi(\gamma(t), T(t))dt + \int_b^{t_0} \psi(\gamma(s), -T(s))ds = u_1(\gamma(t_0)) + u_2(\gamma(t_0)) = u(\gamma(t_0))$. Finally, if $u(\gamma(t)) \neq \min_x u(x)$, then there is a point $y \in \Omega$ with $u(y) < u(\gamma(t))$. However, by Theorem 1 this would mean there is a path from R_1 to R_2 with lower cost than γ, which is a contradiction. □

The properties described in Theorems 1 and 2 all generalize to the high-angular form of (1) so long as the solutions are symmetric, which is guaranteed by $\psi(x, T(x)) = \psi(x, -T(x))$.

2.3 Volumetric Connectivity

Here we define the framework for volumetric connectivity. Let γ be the minimal total cost path, and fix a threshold $\epsilon > 0$, which is the tolerance of paths relative to the optimum. We define an *ϵ-point* as a point whose constrained minimum cost is less than $(1 + \epsilon)E(\gamma)$. The set of all such ϵ-points defines a *volumetric pathway* between R_1 and R_2. This region is the set of voxels that belong to the fiber connection between R_1 and R_2. By definition, a volumetric pathway must contain γ for any value of $\epsilon > 0$. Figure 2 gives a pictoral representation of a volumetric pathway.

The total cost u along a pathway is obviously affected by the Euclidean length of that path. We wish to define a connectivity measure that is independent of the length of a path. Let c_x be the minimal total cost path constrained to pass through the point $x \in \Omega$. By definition, this path has total cost $E(c_x) = u(x)$. As described in Section 3.1, we can solve for $g(x)$, the Euclidean arclength of c_x using a first-order PDE. This allows us to define a *normalized cost* function, $\tilde{u}$, in a volumetric pathway as $\tilde{u}(x) = u(x)/g(x)$. The integral over the ϵ-region of the normalized cost in a volumetric pathway gives a length-invariant measure of the total connectivity of the represented pathway.

2.4 Numerical Implementation

We do not consider the problem of numerical solutions to (4) to be a significant aspect of this paper. However, in the analysis of circuits between large sets of cortical regions, the speed of solutions is a consideration, and the availability of the efficient numerical algorithms will be important.

Several options exist to solve (4) for the cost functions u_1, u_2. For instance, the Lax-Friedrichs method used in [13] is stable but excessively diffusive. Tsai et al. [17] propose a Gudonov approximation for the Hamiltonian, which includes one-sided deratives, and a sweeping method for iteratively updating the solution. In this case, the number of sweeps depends on the complexity of the data. We solve (4) using a new numerical method, the Fast Iterative Method (FIM), which solves the general static Hamilton-Jacobi equation using the Gudonov approximation, which gives an explicit solution for the characteristic direction, and thereby does not require differentiating the cost to obtain path lengths. The FIM updates a list of points whose solutions depend on updated points but are not yet final. This list of points is maintained by removing or adding points based on the convergence of the solution and their dependencies on solved points. The method iteratively updates solutions of the points until the list becomes empty. For full details of the FIM algorithm and implementation, see [18]. Because we are only interested in connectivity in the white matter, we use a white matter mask in which to compute the cost function solutions. For improved numerical accuracy we compute the solution on a grid supersampled by two from the original data. Supersampling is done on the original DWI measurements.

3 Nonparametric Regression of Path Data

Identifying white matter fiber connections as volumetric pathways leaves us with a collection of unparameterized voxels, defined on the original DTI grid, each of which contains information on the tensor, path cost, path length, and path orientation. This collection of raw voxel data offers several possibilities for quantification of the tensor data along these paths. One interesting possibility is the set of integral properties such as average FA, connectivity, etc. In this section we describe a nonparametric regression method for generating a compact statistical description of diffusion tensor data as a function of position along a fiber pathway. The first step is to compute a parameter s for each voxel in the pathway, which is the Euclidean arclength along the minimal cost curves. This arclength will serve as the independent variate in a nonparametric regression of the tensor data along the pathway. Using this regression, we compute mean and variance statistics along fiber pathways of the full diffusion tensor data as well as derived measurements, without any explicit integration of paths.

3.1 Solving for Distance Along Paths

For a given pathway we wish to find the Euclidean arclength along the constrained minimum cost paths between regions R_1 and R_2. We do this by solving a first-order, linear PDE that results in distance along the minimal path to individual targets. If $g_1(x)$ denotes Euclidean arclength along a minimal cost path from R_1 to the point x, it satisfies the advection equation

$$\nabla g_1 \cdot T_1 = 1, \tag{5}$$

where T_1 is the unit length tangent vector to the minimal path connecting each point in Ω to R_1. Likewise for g_2, T_2, R_2, and u_2. There are two possible strategies for evaluating the tangents, T_1. One strategy is the use the characteristics of u_1, which are given by $T_1 = M^{-1}\nabla u_1$, where ∇u_1 is approximated with finite differences, as described in [13]. Alternatively, the Gudonov approximation given in [17], which we use for this paper, requires an explicit calculation of the characteristic direction at each iteration. For this work, we save these vectors, after the solution has converged, and use them for T_1 in Eq. 5.

To solve (5), we use an iterative, fixed point strategy with an up-wind approximation of the gradient of g_1. The initial solution for g_1 is set to a Manhattan distance computed on the set of points for which the speed function is nonzero. It typically converges in several dozen iterations.

In this way, we can also compute the Euclidean arclength, $g_2(x)$, of the minimial cost path from R_2 to the point x. Summing these two distances, g_1 and g_2, we get the total arclength of the minimal cost path from R_1 to R_2 that is constrained to pass through the point x. We denote this total arclength as $g = g_1 + g_2$. The parameter that we use for the dependent variable in our regression is $s = g_1/g$, the percentage of arclength along the minimal cost path from R_1 to R_2. As such, the parameter s takes values in $[0, 1]$.

3.2 Path Regression

Let P be a volumetric pathway, and let $\{x_i\}_{i=1}^N$ be the collection of voxel locations within P. Each voxel has an associated parameter $s_i = s(x_i)$, as defined abovve. Denote by f_i a data value at the location x_i. This data may be a diffusion weighted value, a full diffusion tensor, or a derived measure, such as FA or MD. We compute a continuous description of the data as a function of s using a Nadaraya-Watson nonparametric regression [19,20] with a Gaussian kernel.

$$f(s) = \frac{\sum_{i=1}^N f_i G(s - s_i, \sigma)}{\sum_{i=1}^N G(s - s_i, \sigma)}, \tag{6}$$

where $G(\mu, \sigma)$ denotes a Gaussian with mean μ and standard deviation σ. We choose the kernel width σ used in the regression equation automatically, by minimizing the sum-of-squares cross-validation error. We solve this optimization using a Golden Ratio search. Typical values for the optimal σ are 1–4% of the path length. The function f defined above gives a continuous average of the data along the pathway. Given this mean function, we can use the same regression to estimate the variance of the data along the path:

$$\sigma_f^2(s) = \frac{\sum_{i=1}^N (f_i - f(s))^2 G(s - s_i, \sigma)}{\sum_{i=1}^N G(s - s_i, \sigma)}. \tag{7}$$

In addition to computing diffusion properties along a pathway, it is also possible to statistically quantify the geometry of the path in a similar fashion. Using

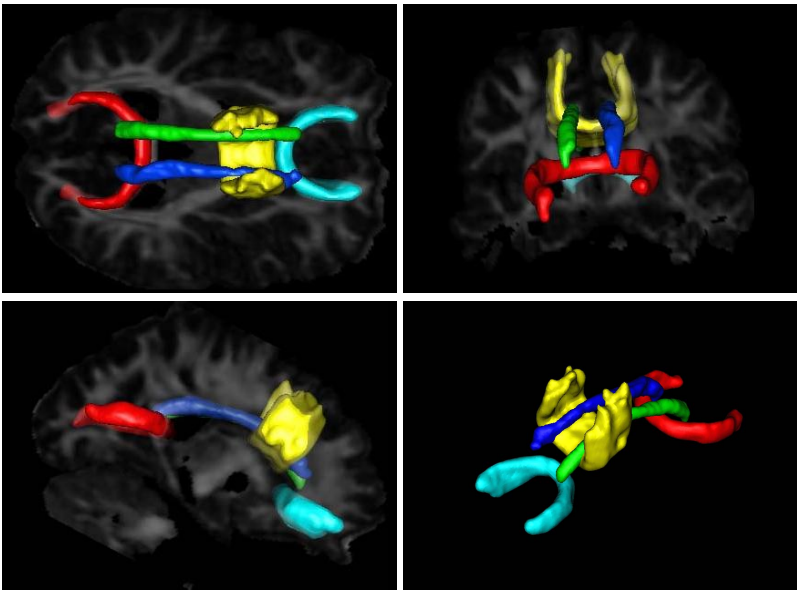

Fig. 3. Volumetric pathways for the GCC (cyan), BCC (yellow), SCC (red), LCG (green) and RCG (blue). Axial, coronal and sagittal views are shown against FA slices.

(6), we can compute the average voxel position along a pathway as a function of s. This results in an curve $(x(s), y(s), z(s))$, which represents the average geometry of the fibers in the connection. Once again, the σ is determined through optimality of the cross validation.

4 Results

We apply our quantitative DTI connectivity analysis to a single high-resolution ($2 \times 2 \times 2.5\text{mm}^3$) 3T image from a database of healthy controls. We selected five tracts for analysis: three bundles through the genu (GCC), splenium (SCC), and body (BCC) of the corpus callosum, and the left (LCG) and right (RCG) cingulum bundles. Using the FA image, we outlined the terminal regions R_1 and R_2 at the white/grey matter interface for each tract. An example of the segmented regions is shown in Figure 1.

For each of the five tracts, we solved for the total cost function u as described in Section 2.3. We chose an ϵ value of 0.10, i.e., we included voxels in the volumetric pathway within $\pm 10\%$ of the optimal total cost curve. Figure 3 shows the resulting volumetric pathways for the five tracts. Next we quantified the FA along each pathway using the nonparametric regression analysis. Figure 4 shows the original raw FA data from all the voxels included in the GCC volumetric pathway and also the mean and standard deviation result from the regression. The regression analysis for the FA of the other four tracts is shown in Figure 5.

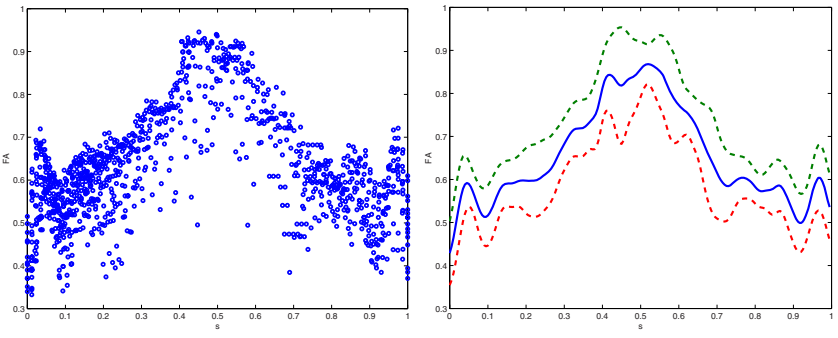

Fig. 4. FA along the GCC: (a) scatterplot of raw data, and (b) nonparametric regression. The solid curve shows average FA, and dashed curves show standard deviation.

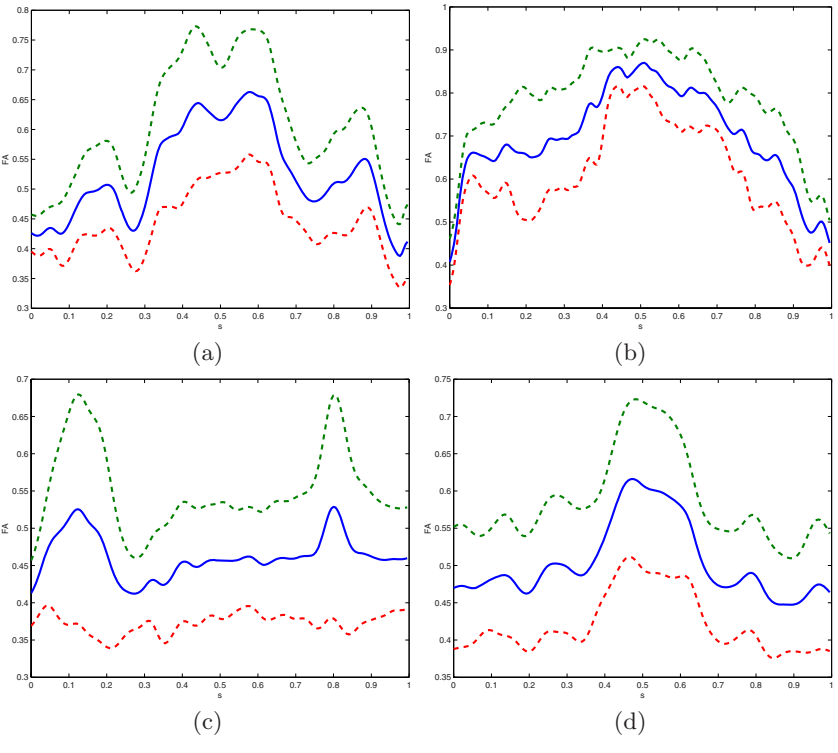

Fig. 5. Nonparametric regression of FA along the (a) BCC, (b) SCC, (c) LCG, and (d) RCG

Notice the similar pattern in each of the corpus callosum pathways, where the FA increases as it passes through the tightly packed fibers of the corpus callosum. In Table 1 we show the aggregate connectivity measurements for each tract,

Table 1. Mean connectivity metrics, normalized cost and alignment, for the five tracts

Measure	GCC	BCC	SCC	LCG	RCG
Norm. Cost	10.8	16.1	7.5	22.8	18.6
Alignment	0.797	0.789	0.708	0.611	0.788

Fig. 6. Average diffusion tensors along the pathways displayed on the average fiber geometries. Rendered using superquadric glyphs [21].

including the average normalized cost $\tilde{u}$, and the average alignment, i.e., dot product, of the major tensor eigenvector and the tangent of the optimal curve at each voxel. Notice that the tracts through the corpus callosum, which have higher anisotropy, also have lower normalized cost (higher connectivity) than the cingulum tracts. The connectivity of the cingulum tracts is also reduced due to partial voluming with the adjacent corpus callosum tensors. Finally, we computed the average positions and average diffusion tensors along each tract, resulting in compact average fiber descriptions, shown in Figure 6.

Acknowledgement

This work is part of the National Alliance for Medical Image Computing (NAMIC), funded by the National Institutes of Health through the NIH Roadmap for Medical Research, Grant U54 EB005149. This work was made possible in part by software from the NIH/NCRR Center for Integrative Biomedical Computing, P41-RR12553-07. Additional funding was provided by Exxon-Mobil Upstream Research and Development. We thank Dr. Janet Lainhart, Dr. Andrew Alexander, Dr. Erin Bigler, and Molly DuBray, of NICHD U19 HD35476 (Neuroimaging component) and the Collaborative Program of Excellence in Autism for their practical support. We thank Dave Weinstein for help in creating visualizations using SCIRun [22], which was used in Figures 3 and 6.

References

1. Kubicki, M., Westin, C.F., Maier, S.E., Mamata, H., Frumin, M., Ernst-Hirshefeld, H., Kikinis, R., Jolesz, F.A., McCarley, R.W., Shenton, M.E.: Diffusion tensor imaging and its application to neuropsychiatric disorders. Harvard Review of Psychiatry 10, 234–336 (2002)
2. Lim, K., Helpern, J.: Neuropsychiatric applications of DTI—a review. NMR in Biomedicine 15, 587–593 (2002)
3. Ding, Z., Gore, J., Anderson, A.: Classification and quantification of neuronal fiber pathways using diffusion tensor MRI. Magnetic Resonance in Medicine 49, 716–721 (2003)
4. Jones, D., Catani, M., Pierpaoli, C., Reeves, S., Shergill, S., O'Sullivan, M., Golesworthy, P., McGuire, P., Horsfield, M., Simmons, A., Williams, S., Howard, R.: Age effects on diffusion tensor magnetic resonance imaging tractography measures of frontal cortex connections in schizophrenia. Human Brain Mapping 27, 230–238 (2006)
5. Corouge, I., Fletcher, P.T., Joshi, S., Gouttard, S., Gerig, G.: Fiber tract-oriented statistics for quantitative diffusion tensor MRI analysis. Medical Image Analysis 10(5), 786–798 (2006)
6. Basser, P.J., Pajevic, S., Pierpaoli, C., Duda, J., Aldroubi, A.: In-vivo fiber tractography using DT-MRI data. Magnetic Resonance in Medicine 44, 625–632 (2000)
7. Koch, M.A., Norris, D.G., M, H.G.: An investigation of functional and anatomical connectivity using magnetic resonance imaging. NeuroImage 16, 241–250 (2002)
8. Behrens, T., Woolrich, M., Jenkinson, M., Johansen-Berg, H., Nunes, R., Clare, S., Matthews, P., Brady, J., Smith, S.: Characterization and propagation of uncertainty in diffusion-weighted MR imaging. Magnetic Resonance in Medicine 50, 1077–1088 (2003)
9. Parker, G.J.M., Haroon, H.A., Wheeler-Kingshott, C.A.M.: A framework for a streamline-based probabilistic index of connectivity (PICo) using a structural interpretation of MRI diffusion measurements. Journal of Magnetic Resonance Imaging 18, 242–254 (2003)
10. Lazar, M., Alexander, A.L.: Bootstrap white matter tractography (BOOT-TRAC). NeuroImage 24, 524–532 (2005)
11. Parker, G., Wheeler-Kingshott, C., Barker, G.: Estimating distributed anatomical connectivity using fast marching methods and diffusion tensor imaging. Transactions on Medical Imaging 21, 505–512 (2002)
12. O'Donnell, L., Haker, S., Westin, C.F.: New approaches to estimation of white matter connectivity in diffusion tensor MRI: elliptic PDEs and geodesics in a tensor-warped space. In: MICCAI 2002, pp. 459–466 (2002)
13. Jackowski, M., Kao, C.Y., Qiu, M., Constable, R.T., Staib, L.H.: Estimation of anatomical connectivity by anisotropic front propagation and diffusion tensor imaging. In: MICCAI 2004, pp. 663–667 (2004)
14. Pichon, E., Westin, C.F., Tannenbaum, A.: A Hamilton-Jacobi-Bellman approach to high angular resolution diffusion tractography. In: MICCAI. 2005 180–187 (2005)
15. Lenglet, C., Deriche, R., Faugeras, O.: Inferring white matter geometry from diffusion tensor MRI: application to connectivity mapping. In: ECCV 2004 (2004)
16. Beaulieu, C.: The basis of anisotropic water diffusion in the nervous system – a technical review. NMR in Biomedicine 15, 435–455 (2002)
17. Tsai, Y., Cheng, L., Osher, S., Zhao, H.: Fast sweeping methods for a class of hamilton-jacobi equations. SIAM Journal of Numerical Analysis 41, 673–694 (2003)

18. Jeong, W.K., Whitaker, R.: A fast iterative method for eikonal equations. Technical report, Scientific Computing and Imaging Institute, University of Utah (2007)
19. Nadaraya, E.A.: On non-parametric estimates of density functions and regression curves. Theory of Probability and its Applications 10, 186–190 (1965)
20. Watson, G.S.: Smooth regression analysis. Sankhy'a Ser. A 26, 101–116 (1964)
21. Kindlmann, G.: Superquadric tensor glyphs. In: Proceedings of IEEE TVCG/EG Symposium on Visualization 2004, pp. 147–154 (2004)
22. SCIRun: A scientific computing problem solving environment, Scientific Computing and Imaging Institute (SCI), `http://software.sci.utah.edu/scirun.html`